ELSEVIER

Biophysical Chemistry 103 (2003) 13–23

Biophysical Chemistry

www.elsevier.com/locate/bpc

NMR study of the conformational transition of cytochrome *c* upon the displacement of Met80 by exogenous ligand: structural and magnetic characterization of azidoferricytochrome *c*

Yong Yao[a], Yibing Wu[a], Chengmin Qian[a], Keqong Ye[b], Jinfeng Wang[b], Wenxia Tang[a,*]

[a]*State Key Laboratory of Coordination Chemistry, Nanjing University, Nanjing 210093, PR China*
[b]*National Laboratory of Biomacromolecules, Institute of Biophysics, Academic Sinica, Beijing 100101, PR China*

Received 22 March 2002; received in revised form 22 May 2002; accepted 23 May 2002

Abstract

As the exogenous ligand–cytochrome *c* complexes were purported to represent models for the unfolding intermediate of cytochrome *c*, NMR spectroscopy has been utilized to study the azide adduct of horse heart cytochrome *c*. The structure of azidoferricytochrome *c* was modeled by restrained energy minimization using paramagenetic pseudocontact shifts as constraints. The bound azide moiety was found to be tilted approximately 15° from the heme normal. The displacement of Met80 by the exogenous azide molecule causes large structural rearrangement in the distal cavity. Furthermore, the conformation transition associated with the swing out of the loop containing Met80 and the shift of the 50s-helix increases the solvent accessibility of the heme group. To elucidate the heme electronic structure of the complex, the paramagnetic ^{13}C shifts were analyzed in terms of a model based on the π molecular orbitals of the heme under perturbed D_4 symmetry. It turned out that the His–Fe bonding provides the protein constraint that orients the in-plane anisotropy in the complex. The electronic properties are in accordance with the calculated magnetic susceptibility anisotropy and the structural information.

Keywords: Cytochrome *c*; Exogenous ligand; Unfolding intermediate; Conformational transition; Electronic structure

1. Introduction

Cytochrome *c* (cyt *c*), which shuttles electrons from cytochrome *c* reductase to cytochrome *c* oxidase during aerobic respiration, is one of the most extensively studied hemoproteins [1–8]. The structure of native cyt *c* has been well characterized by both X-ray crystallography [9–11] and NMR spectroscopy [12–14]. Several unfolded states of the oxidized species have also been detected spectroscopically as a function of temperature, pH and denaturating agents [15–17]. One important feature of cyt *c* folding and unfolding process concerns the involvement of covalently attached heme group and its axial ligands [18–24]. The coordination of His18 and Met80 stabilizes the native state. Under denaturing conditions, His18, remains bound to the heme iron, but the second ligand, Met80, is replaced by a non-native

*Corresponding author. Tel.: +86-25-3595706; fax: +86-25-3314502.
E-mail address: wxtang@netra.nju.edu.cn (W. Tang).

0301-4622/03/$ - see front matter
PII: S0301-4622(02)00141-2

ligand. This ligand was identified as a Lys (species L) under partially denaturing conditions and a His (species H) under strongly denaturing conditions [15,18–24]. To investigate the conformational transition induced by the breakage of Fe–S bond, exogenous ligands like CN^-, NH_3, pyridine and imidazole were used as probes applying spectroscopy methods [25–30]. The resolved solution structure of the imidazole–cyt *c* complex showed that the displacement of Met80 by an exogenous imidazole molecule causes pronounced structural rearrangement in the distal pocket while it maintained the majority of the structure of the native protein [30]. NMR investigation of cyt *c* unfolding showed that species L bears a strong similarity to the cyanide adducts of cyt *c* in the hyperfine shift region and the heme methyl resonances of species H are indeed similar to those observed for the pyridine and imidazole derivatives of cyt *c* [15]. Furthermore, the enthalpy ($\sim$60 kJ/mol) [31] of the conformational transition coupled to the reaction between the exogenous ligands and cyt *c* is comparable to the enthalpy for the partial unfolding of the protein [32]. Hence, the exogenous ligand cyt *c* derivatives could represent a model for the unfolded intermediate of cyt *c* [15,32] and the knowledge of their structures would provide valuable information on the structure and function relationship of this protein.

As a larger linear ligand compared to cyanide, the azide moiety might not bind to cyt *c* perpendicularly and the tilt of the azide molecule may reflect how the topology of the exogenous ligand modulates the heme distal cavity during its interaction with the protein. Up to now, many interests have been focused on the azide complex of ferric cyt *c*, showing that this complex is in the purely low spin state between 20 and 315 K [33–35]. Partial spectroscopic characterization of azidoferricyt *c* has been presented previously [35]. In this work, we extended the assignments of protons to approximately 80% of all residues. The availability of a large number of chemical shifts permits the determination of the magnetic susceptibility anisotropy of this complex [36]. An initial modeling template was constructed from the solution structure of the cyanide–cyt *c* complex and then energy minimized using constraints derived from the pseudocontact shifts. The ^{13}C shifts of the heme methyls and the pro-7α were analyzed in terms of a model based on the π molecular orbitals of the heme under perturbed D_4 symmetry, which yields the orientation of the rhombic perturbation θ and an energy splitting parameter ΔE [37–39]. Analysis of these data and comparison with the structural and magnetic information which is available for cyanoferricyt *c* shows how the nature of the exogenous ligands take effect on the perturbation to the heme cavity and the electronic structure of the heme center in cyt *c* derivatives.

2. Materials and methods

2.1. Sample preparation

Horse heart cyt *c* (Type VI) was purchased from Sigma Chemical Co. and purified as previously described [40]. The ^1H NMR samples were prepared by dissolving the lyophilized protein in 90% H_2O/10% D_2O or D_2O. NaN_3 in pH-adjusted solution was added. The final NMR samples contained 4 mM hh cyt *c* and 1.5–2.5 M NaN_3 at pH or pD 7.0 (uncorrected for the isotope effect).

2.2. NMR spectroscopy

The NMR spectra were collected on Bruker DMX 600 and Bruker DRX 500 spectrometers at 300 and 313 K. The 500 MHz ^1H NMR 1D spectra were recorded using the superWEFT sequence [41] with recycle delay ranging from 33 to 250 ms. 2D DQF-COSY, TOCSY and NOESY spectra were collected following standard pulse sequences [42]. NOESY maps in D_2O solution were recorded on a spectral width of 30 ppm with a recycle time of 600 ms and a mixing time of 50 ms. To optimize the observation of connectivities in the diamagnetic region, NOESY maps in H_2O solutions were recorded on a smaller spectral width (16 ppm), with recycle time of 1.2 s and mixing times of 70–120 ms. Analogously, TPPI DQF-COSY and TPPI clean TOCSY experiments were recorded over the spectral width of 16 ppm (recycle time of 1.2 s and spin lock times of 40–80 ms).

The $^{1}H-^{13}C$ HMQC spectra were carried out using natural abundance samples without decoupling during acquisition. The Δ delay was adjusted to optimize sensitivity according to the line widths of heme methyl signals. The chemical shifts were calibrated in the proton frequency using water as internal reference and in the carbon frequency using dioxane at 66.6 ppm.

Data processing was performed using the standard Bruker software package XWINNMR [43] on a Silicon Graphics workstation, the 2D spectra were analyzed with the aid of the program XEASY [44].

2.3. Structure modeling strategy

Since the ion strength of the sample is very high, calculation of a solution structure of azide–cyt *c* by conventional NOE constraints has been hampered by the poor quality of the NOESY spectra. The relationship between pseudocontact shift (δ_{pc}) and coordinates of a proton within the molecular axes is well known [45]:

$$\delta_{pc}=\frac{1}{12\pi r^3}\left[\Delta\chi_{ax}(n^2-1)-\frac{3}{2}\Delta\chi_{rh}(l^2-m^2)\right] \quad (1)$$

where $\Delta\chi_{ax}$ and $\Delta\chi_{rh}$ are the axial and rhombic magnetic susceptibility anisotropics, *r* is the length of the metal–nucleus vector, and *l*, *m* and *n* are the direction cosines of the vector. As the pseudocontact shifts contain structural information, they could be utilized as long-range constraints to refine the structures of both proteins and nuclear acids [46–50]. In this paper, we modeled the solution structure of the present complex according to the following procedure: (1) building a starting structure from the homologous construction; (2) determination of the χ tensor anisotropy parameters from the starting structure; (3) recalculation of a new structure by pseudocontact shifts constraints; (4) redetermination of the χ tensor anisotropy parameters from the new structure, and so on, until self-consistency.

2.4. Fit of the ^{13}C paramagnetic shifts

In a six-coordinated ferricheme with D_{4h} symmetry, the frontier molecular orbitals of the heme form a pair of π orbitals ϕ_x and ϕ_y which are dominated by the metal d_{xy} and d_{yz} atomic orbitals. The protein environment introduces a rhombic perturbation at some arbitrary angle with respect to the iron-centered reference coordinate system and therefore resolves the degeneracy of the ground state of heme iron to give molecular orbitals Φ_x and Φ_y. The Fermi contact shift of the carbon nuclei in positions α to the tetrapyrrole ring may be expressed as [37,45]:

$$\delta_{\mathrm{con}}=\frac{2\pi g_e\beta_e S(S+1)Q\rho_i}{3kT\gamma} \quad (2)$$

where β_e is the Bohr magneton, *Q* is the hyperfine coupling parameter, γ is the nuclear magnetogyric ratio and ρ_i is the unpaired electron spin density on the *i*th pyrrole β carbon. The parameter ρ_i is defined with respect to a simple Boltzmann distribution of the unpaired electron in the two splitted orbitals Φ_x and Φ_y [37,45]:

$$\rho_i=c^2_{\Phi xi}+\varepsilon c^2_{\Phi yi}/(1+\varepsilon);\quad \varepsilon=\exp(-\Delta E/RT)$$
$$|\Phi_x\geqq\sin\theta|\phi_x>-\cos\theta|\phi_y>;$$
$$|\Phi_y\geqq\sin\theta|\phi_x>+\cos\theta|\phi_y> \quad (3)$$

where θ is an angular orbital mixing parameter defined as the angle of the orientation of the rhombic perturbation counterclockwise to the vector connecting the Fe and NB, and ΔE is the empirical energy splitting of the orbitals ($\Delta E=E_{\Phi y}-E_{\Phi x}$).

The ^{13}C paramagnetic shifts of substituents α to the heme obtained at two temperatures were fitted to the model with correction for pseudocontact contributions. The ^{13}C shifts of the reduced horse cyt *c* were used as the diamagnetic reference. The two molecular orbital coefficients were fixed at the values obtained in native horse cyt *c* [37]. The values of ΔE, θ and the hyperfine coupling parameter *Q* were treated as variables in the analysis.

3. Results and discussions

3.1. Chemical shifts assignment

Resonance assignments were obtained by standard procedures [42]. The chemical shifts of the assigned protons are listed in Table S1 in the supplementary material. The heme resonances

Table 1
Chemical shifts of some paramagnetic resonances in azide-cyt *c*

	Chemical shifts (ppm)			
	300 K		315 K	
	^{1}H	^{13}C	^{1}H	^{13}C
1-CH_3	15.1	−31.1	14.9	−27.0
3-CH_3	4.6	−2.7	5.9	−0.3
5-CH_3	17.5	−31.5	17.3	−28.4
8-CH_3	16.7	−36.1	16.0	−31.8
Thioether-2	0.5	n.d.	0.7	n.d.
Pro-7α	−0.3	n.d.	0.5	7.1
	−0.3		0.5	
His18α	8.5	73.8	8.4	72.8
His18β	11.3	23.3	11.0	26.6
	6.0		6.1	
His18ε_1	−9.0	n.d.	−7.2	n.d.

were assigned by use of a combination of data from EXSY [35], NOESY and HMQC experiments. The positions of the αCH and βCH_2 protons of His18 were confirmed by their characteristic pattern in the TOCSY and HMQC spectra. The Hε1 of His18 was identified in the ID superWEFT spectrum with a recycle delay of 33 ms and a τ delay of 45 ms. The assigned paramagnetical resonances are reported in Table 1.

3.2. Pseudocontact shifts constraints

The pseudocontact shifts were determined by subtracting the chemical shifts measured in the reduced species of the native enzyme [14] from those of the present azide bound oxidized species. The amide shifts were not included because they are sensible to the solution environment. The shifts of residues that can contain non-negligible contact shift contributions such as the heme, histidine 18, cysteine 14 and 17, were not included. In total, 144 pseudocontact shifts were used as constraints during the energy minimization.

As the preliminary of the use of pseudocontact shifts constraints was a safe estimate of the pseudocontact shifts, the problem arose of finding an ideal diamagnetic reference. Indeed, no such ideal reference diamagnetic protein exists, because any diamagnetic reference must be in the reduced state and may be structurally different, in some details, from the actual oxidized compound. The difference is even large in the present case, due to the displacement of the axial ligand by an exogenous one. Relaxing the conditions of the acceptance of a diamagnetic reference makes the approach more general [49,50]. In this respect, a tolerance of 10% of the observed pseudocontact shifts was used with a minimum value of 0.3 ppm [12,27,30]. For the protons of residues 70–85 where major structural rearrangements are expected, the tolerance was set to 0.8 ppm and the proton shifts of residues 78–82 were excluded during calculation.

3.3. Structural modeling

The high-resolution solution structure of cyanoferricyt *c* (PDB entry 1I5T) [27] was used for initiation of model construction. The cyanide moiety was replaced by an azide molecule with the potential energy parameters and partial charges calculated by the program SYBYL [51]. The bond angle Fe–N1=N2 was varied between 120 and 180°, and the Fe–N1 bond could rotate freely during the energy minimization to look for a best orientation of the azide moiety. Molecular modeling was performed with the SANDER module in AMBER package [52] on an SGI O2 workstation. The total energy was minimized via mechanics by using a steepest descent algorithm and a subsequent conjugate gradient method. After the first circle of energy minimization, the resulting structure was used to fit the pseudocontact shifts to determine the magnetic susceptibility anisotropy by the program FANTASIAN [50]. Then, the five parameters of the magnetic susceptibility anisotropy and the pseudocontact shifts constraints were included as structural restraints during a new cycle of energy minimization using the resulting structure as starting template. A force constant of 100 kcal mol^{-1} ppm^{-2} was used during the REM calculation. This procedure was repeated until no variation in the values of both $\Delta\chi_{ax}$ and $\Delta\chi_{rh}$. In each cycle, the decrease in energy during the minimization routine was monotonous. Thus, it is not necessary to use dynamics simulations. The final structure of the azide–cyt *c* complex was illustrated in Fig. 1.

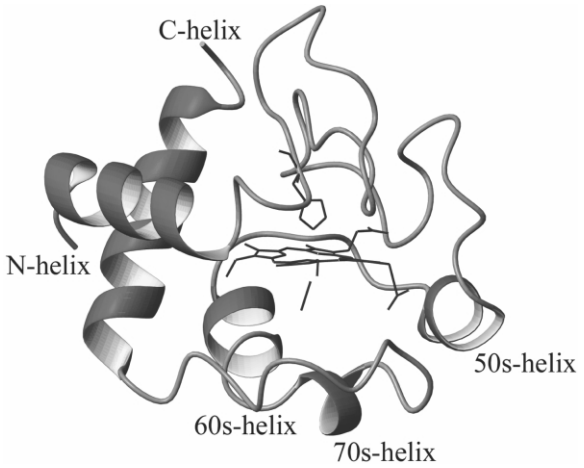

Fig. 1. The secondary structure and overall fold of the azide adduct of oxidized horse heart cytochrome *c*.

To test the convergence of the structure calculated by the pseudocontact shifts constraints, a family of 35 structures was also calculated using the structure family of cyanoferricyt *c* as starting templates applying the same method. The final family has RMSD values of 0.54 ± 0.08 Å for backbone and 1.13 ± 0.10 Å for all heavy atoms. For residues 75–85 where large structural rearrangement is expected, the RMSD value is 0.78 Å for the backbone atoms.

3.4. Structural analysis

Comparison of the structure of the azide–cyt *c* with the reported solution structure of the native protein (PDB entry 1AKK) [12] shows that that all elements of helical structures are well conserved in the present structures (Fig. 1). However, remarkable structure change occurs in the distal cavity. Met80 is now pointing away from the center of the cavity towards the outside. The induced structural rearrangements propagate and have a major influence on nearby residues. The backbone of residues 77–85 is shifted away from the heme and a concomitant shift of the 50s-helix is noted (Fig. 2), hence, resulting in a close-open transition of the heme crevice. The similar conformation transition is also observed in other ligand cyt *c* complexes [27,30] and thus, may reflect the common structure change upon the displacement of Met80 by exogenous ligands.

Fig. 2. The superimposed structures of the native horse heart cytochrome *c* and the azide–cytochrome *c* complex. Helices are represented by cylinders. Black represents the native horse heart cytochrome *c* and light grey represents the azide adduct of oxidized horse heart cytochrome *c*. The figure was created with the program MOLMOL [56].

As a large linear ligand, the azide moiety is tipped $\sim 15^\circ$ from the heme normal and the projection of the azide molecule on the heme is approximately along the Fe–NA direction (Fig. 3). This is different from the cases in cyanide–cyt *c* complexes, in which it was believed that the cyanide molecule bound perpendicularly to the heme [25,27]. The structural changes in the distal pocket associated with the displacement of the distal ligand from cyanide to azide are illustrated in Fig. 4. It can be noted that Tyr67 in azide–cyt *c* moves outward from the heme to accommodate the larger azide molecule. Another noticeable difference concerns the movement of Phe82 and a rotation of its aromatic ring. It has been pointed out that Phe82 is sensible to the conformational transition involving the change of the distal ligand [53,54].

4. Magnetic susceptibility tensor

The tensor has $\Delta\chi_{ax}$ and $\Delta\chi_{rh}$ values of 3.35×10^{-32} and 1.47×10^{-32} m^3, respectively.

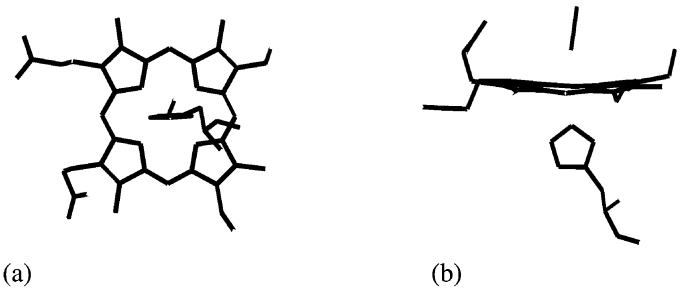

Fig. 3. (a) Face-on view and (b) edge-on view of the orientation of the azide molecule in the azide adduct of oxidized horse heart cytochrome *c*.

The principal *z*-axis of the magnetic anisotropy tensor forms an angle of 13° with the perpendicular to the heme plane and the *x*-axis forms an angle of 52.4° clockwise to Fe–NB (pyrrole II) direction.

The orientation of the magnetic anisotropy tensor is directly linked to the orientation of the two axial ligands according to the counter-rotation rules [45]. Although the bound azide molecule is tipped ~15° from the heme normal, it is still reasonable to predict that the His18 plane determines the in-plane anisotropy as the case in cyanide–cyt *c* complex [27]. In the modeled solution structure of azide–cyt *c*, the His18 plane makes an angle of 48.3° counterclockwise to the Fe-pyrrole II nitrogen direction, which is in agreement with our observed value of 52.4° of the angle of the *x*-axis of magnetic susceptibility.

For comparison purposes, it is reminded that the parameters for CN-Met80Ala cyt *c* [49,50] and cyanoferricyt *c* [27] are 3.30×10^{-32} and 3.68×10^{-32} m^3 for $\Delta\chi_{ax}$, and 0.73×10^{-32} and 0.84×10^{-32} m^3 for $\Delta\chi_{rh}$.

4.1. Characterization of the heme electronic structure

^{13}C paramagnetic shifts tend to be more symmetrical than those of protons [39]. This is evident in these data (Table 1), with a ratio of 1.2 between

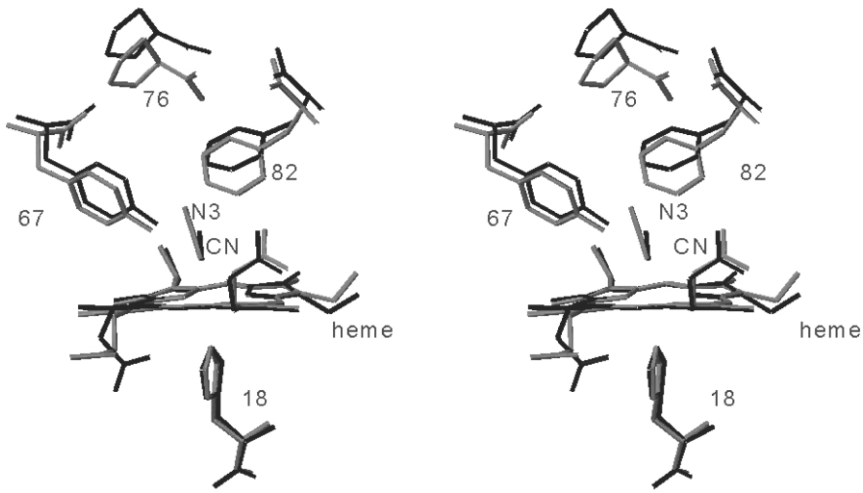

Fig. 4. A stereoview of the superimposed structure of cyanide–cytochrome *c* complex (black) and the cyanide–cytochrome *c* complex (grey).

Table 2
Summary of parameters obtained by fitting ^{13}C Fermi contact shifts in cyt *c* and its derivatives

	θ (°)	ΔE (KJ mol^{-1})	Q (MHz)
Cyt *c*[37]	84.3	−5.14	−39.0
Cyanide-cyt *c* [55]	49.4	−2.30	−37.4
Azide-cyt *c*	47.8	−3.82	−23.8

the shifts of 1-CH_3 and 5-CH_3 protons, but a ratio of only 1.0 between the methyl carbons. The fitted three parameters ΔE, θ and Q are listed in Table 2 and the parameters for native cyt *c* and cyanide–cyt *c* are also include. It can be noticed that the rhombic perturbation in cyanide–cyt *c* and azide–cyt *c* are quite similar, and the two complexes are significantly different from the native protein, indicating that the bind of non-native exogenous ligand alters the electronic structure of the heme.

The orientation of the rhombic perturbation (θ) is related directly to the in-plane orientation of the magnetic axis and to the geometry of both axial ligands with respect to the heme [45]. In the present complex, the parameter θ (47.8°) has been shown to be similar to the rotation of the χ_x magnetic axis (52.4°) projected on the heme plane, but of opposite direction. It is interesting to note that the projection of the His18 imidazole ring onto the heme plane (an angle of 48.3° counterclockwise to the Fe–NB direction) align closely to the rhombic perturbation θ. This confirms the idea that the His–Fe bonding provides the protein constraint that orients the in-plane anisotropy in the azide–cyt *c* complex, similar to the case in the cyanide–cyt *c* adduct.

The parameters characterizing the heme electronic structure of native cyt *c* and some ligand–cyt *c* complexes are listed in Table 3. It can be noted that the orientations of the axial ligands align closely with the rhombic perturbation. The pattern of the hyperfine-shifted resonances of porphyrin methyl protons are determined by the orientation of the axial ligands and consequently, the rhombic perturbation [45]. In native cyt *c*, both the His18 and the Met80 are contributing and give a rhombic perturbation of approximately 85° [37]. As studied previously, this value gives rise to a pairwise pattern to the heme methyls on opposite pyrrole rings, the 8-CH_3 and 3-CH_3 having significant larger shifts than 5-CH_3 and 1-CH_3 [45]. As cylindrical symmetry ligands, cyanide and azide do not perturb the π orbital of the heme (although a tilt of the azide moiety from the heme normal is observed in the modeled structure). Thus, in the two complexes only the orientation of the p_π orbital of the His ring defines the shift pattern. The rhombic perturbation of the two complexes was close to the β/δ meso directions. It is then expected that the spin density is distributed comparably to the four methyls in the two complexes. This agrees with the result that these two cyt *c* derivatives have similar hyperfine shift pattern, and the lowest spin density is located in 3-CH_3. However, a noticeable difference between the cyanide–cyt *c* and azide–cyt *c* can also be noted. It is observed that the chemical shift values of the methyl shifts (both proton and carbon) in azide–cyt *c* are significantly smaller than their corresponding values in cyanide. This could be rationalized as a result of a drop of value of the hyperfine coupling constant Q in azide–cyt *c* (Table 2).

Acknowledgments

We express our thanks to Prof. Ivano Bertini of University of Florence, Italy, for his kind provision

Table 3
Chemical shifts for the heme methyl groups, axial ligands orientation and rhombic perturbation for cyt *c* and its derivatives

	Heme methyls shifts pattern	Proton chemical shifts (ppm)				Axial ligands orientation	Rhombic perturbation (θ)
		1-CH_3	3-CH_3	5-CH_3	8-CH_3		
Cyt *c*[12,37]	8>3≫5>1	7.1	38.7	10.2	34.5	39° (His18) 93° (Met80)	85°
Cyanide-cyt *c*[27,11]	5>8>1>3	16.6	11.4	23.1	21.5	42° (His18)	47°
Azide-cyt *c*	5>8>1>3	15.1	4.6	17.5	16.7	48° (His18)	49°

of the program FATANSIAN. This project was supported by the National Natural Science Foundation of China, the Natural Science Foundation of Jiangsu Province and the Foundation of the Education Administration.

Appendix A: Table S1. Chemical shifts of diamagnetic protons of azide-cyt *c* at 300 K and pH 7.0

	NH	Hα		HB		Others
Glyl	8.11	3.90	3.58			
Asp2	9.23	4.65		2.72	2.39	
Val3	8.35	3.46		2.08		γCH3 1.00 0.96
Glu4	7.99	4.00		2.07		Hγ2.30
Lys5	7.82	3.92		1.69		Hγl.41
Gly6	8.63	3.91	3.29			
Lys7	7.94	2.20				
Lys8	6.87	3.91		1.87		Hγl.37 Hδ 1.67 1.58 Hε 2.94
Ile9	7.66	3.62		1.76		γCH_3 0.73
Phe10	8.43	3.53		3.03	2.65	
Val11	8.75	3.65		2.20		γCH_3 1.21 1.01
Gln12	7.89	4.11		2.21	2.15	Hγ 2.56 2.40
Lys13	8.64	4.57		2.41	1.43	
Cys14	8.00					
Ala15	7.69	5.14		1.81		
Gln16	9.08	4.28		2.19	1.82	
Cys17	8.14					
His18	9.85	8.51		11.36	6.04	$H\varepsilon_1$ –9.05
Thr19	10.21	5.70		5.22		γCH_3 2.05
Val20	8.83	4.59		1.84		γCH_3 0.72 0.47
Glu21	8.44	4.45		2.42	2.12	
Lys22	8.84	3.40		1.45	1.17	Hγ 0.57
Gly23	9.39	4.10	3.80			
Gly24	8.19	4.20	3.65			
Lys25	8.71	4.34		2.12	2.02	Hγ 1.74
His26	8.98	5.48		4.22	3.48	$H\delta_2$ 7.31
Lys27	8.80	4.95		2.44		Hγ 2.04 1.74
Thr28		3.60		3.24		γCH_3 0.16
Leu32						Hγ 3.18 δCH_3 1.90 1.74
His33	7.98	3.87		3.20	3.25	$H\delta_2$ 7.42
Gly34	8.73	3.96	3.67			
Leu35	6.95	3.31		1.85	1.76	Hγ 0.51 δCH_3 –0.24 –0.51
Phe36	8.35	3.63		3.00		Hδ 7.09 Hε 6.56 Hη 6.41
Gly37	8.16	4.30	3.46			
Arg38	8.01	4.76		1.51		
Thr40	7.40					γCH_3 0.72
Ala43	8.30	4.55		1.52		
Phe46				3.46	2.63	Hδ 6.78 Hε 6.36
Thr47	7.07	4.14		3.54		γCH_3 0.95
Tyr48	8.22	4.56		3.31	2.63	Hδ 7.29 Hε 6.95
Thr49	8.62	4.22		4.46		γCH_3 1.31
Asp50	7.83	4.34		2.63	2.58	
Ala51	7.83	4.08		1.41		
Asn52	8.14	4.38		2.92	2.82	
Thr58	7.97	4.03		3.63		γCH_3 0.85
Trp59	8.66	4.43				$H\delta_1$ 6.46 $H\varepsilon_3$ 6.65 $H\zeta_3$ 6.08 $H\zeta_2$ 6.94 Hη 6.34

(Continued)

	NH	Hα		HB		Others
Lys60	7.79	4.30		1.92		
Glu61	9.82	3.59		2.22	2.02	Hγ2.34
Glu62	9.23	3.96		1.95	2.02	Hγ2.34
Thr63	6.95	4.21		4.30		γCH_3 1.27
Leu64	8.48	3.78		1.40		Hγ 1.07 δCH_3 −0.50 −0.79
Met65	8.16	3.78		2.20	2.00	Hγ 2.60 2.55
Glu66	6.68	4.17		1.84		Hγ 2.42 2.20
Leu68	8.24			1.42	0.75	Hγ 1.14 δCH_3 −1.13 −1.18
Glu69	7.16	4.22		2.21		Hγ 2.36
Tyr74	8.23	4.77		3.79	2.63	Hγ 7.65 Hε 6.75
Lys79	8.32	4.38		1.69		Hγ 1.85
Ile81		2.57		2.48		Hγ 1.36 0.50 δCH_3 0.27
Phe82						Hδ 7.99 Hε 7.31 Hη 6.96
Ala83	8.63	4.72		1.76		
Gly84	8.84	4.30	3.88			
Ile85	7.97	4.31		1.68		γCH_3 0.87 Hγ 1.32 1.17 δCH_3 0.59
Lys87	8.42	4.58		2.83	2.75	
Lys88	8.54	4.16		1.91	1.76	Hγ 2.00
Thr89	8.32	3.98		4.11		γCH_3 1.28
Glu90	6.32	4.08		2.23		
Arg91	7.40	3.47		2.04	1.99	Hγ 1.65 0.93 Hδ 1.73
Glu92	8.32	3.52		2.04		
Asp93	8.22	4.07		2.50		
Leu94	8.07	3.86		1.61	1.41	Hγ 1.00 δCH_3 0.73 0.46
Ile95	8.45	3.08		1.69		γCH_3 0.77 Hγ 1.04 δCH_3 0.85
Ala96	7.72	3.86		1.22		
Tyr97	7.86	4.10		3.47	2.78	Hδ 7.06 Hε 6.25
Leu98	8.70	3.12		1.64	0.75	Hγ 1.44 δCH_3 −0.02 −0.36
Lys99	8.65	2.58		1.37	1.14	Hγ 0.52 0.23 Hε 2.49
Lys100	6.69	4.00		1.69		Hγ 1.36
Ala101	8.49	3.90		0.57		
Thr102	7.72	4.30		4.62		γCH_3 0.88
Asn103	6.90	4.77		2.76	2.52	
Glu104	7.54	4.19		2.05	1.97	Hγ 2.30

References

[1] G.R. Moore, G.W. Pettigrew, Cytochrome *c*, Evolutionary Structural and Physiological Aspects, Springer-Verlag, Berlin, 1990.

[2] R.A. Scott, A.G. Mauk, Cytochrome *c*, a Multidisciplinary Approach, University Science Books, Sausalito, 1996.

[3] P. Mulligan-Pullyblank, J.S. Spitzer, B.M. Gilden, J.S. Fetrow, Loop replacement and random mutagenesis of omega-loop D, residues 70–84, in *iso*-L-cytochrome *c*, J. Biol. Chem. 271 (1996) 8633–8645.

[4] S.M. Baxter, J.S. Fetrow, Hydrogen exchange behavior of [U-^{15}N]-labeled oxidized and reduced *iso*-L-cytochrome *c*, Biochemistry 38 (1999) 4493–4503.

[5] J.S. Fetrow, S.M. Baxter, Assignment of ^{15}N chemical shifts and ^{15}N relaxation measurements for oxidized and reduced *iso*-L-cytochrome *c*, Biochemistry 38 (1999) 4480–4492.

[6] A.K. Bhuyan, J.B. Udgaonkar, Stopped-flow NMR measurement of hydrogen exchange rates in reduced horse cytochrome *c* under strongly destabilizing conditions, Proteins 32 (1998) 241–2477.

[7] D.R. Hostetter, G.T. Weatherly, J.R. Beasley, et al., Partially formed native tertiary interactions in the A-state of cytochrome *c*, J. Mol. Biol. 289 (1999) 639–644.

[8] P.D. Barker, I. Bertini, R. Del Conte, et al., A further clue to understanding the mobility of mitochondrial yeast cytochrome *c*. A ^{15}N $T_{1\rho}$ investigation of the oxidized and reduced species, Eur. J. Biochem. 268 (2001) 4468–4476.

[9] G.V. Louie, G.D. Brayer, High-resolution refinement of yeast *iso*-L-cytochrome *c* and comparisons with other

eukaryotic cytochromes *c*, J. Mol. Biol. 214 (1990) 527–555.
[10] G.W. Bushnell, G.V. Louie, G.D. Brayer, High-resolution three-dimensional structure of horse heart cytochrome *c*, J. Mol. Biol. 214 (1990) 585–595.
[11] A.M. Berghuis, G.D. Brayer, Oxidation state-dependent conformational changes in cytochrome *c*, J. Mol. Biol. 223 (1992) 959–976.
[12] L. Banci, I. Bertini, H.B. Gray, et al., Solution structure of oxidized horse heart cytochrome *c*, Biochemistry 36 (1997) 9867–9877.
[13] L. Banci, I. Bertini, T. Reddig, P. Turano, Monitoring the conformational flexibility of cytochrome *c* at low ionic strength by ^{1}H-NMR spectroscopy, Eur. J. Biochem. 256 (1998) 271–278.
[14] L. Banci, I. Bertini, J.G. Huber, G.A. Spyroulias, P. Turano, Solution structure of reduced horse heart cytochrome *c*, J. Biol. Inorg. Chem. 4 (1999) 21–31.
[15] B.S. Russell, R. Melenkivitz, K.L. Bren, NMR investigation of ferricytochrome *c* unfolding: detection of an equilibrium unfolding intermediate and residual structure in the denatured state, Proc. Natl. Acad. Sci. USA 97 (2000) 8312–8317.
[16] D.S. Cohen, W. Pielak, Stability of yeast *iso*-L-ferricytochrome *c* as a function of pH and temperature, Protein Sci. 3 (1994) 1253–1260.
[17] L. Wang, R.X. Chen, N.R. Kallenbach, Proteolysis as a probe of thermal unfolding of cytochrome *c*, Proteins 30 (1998) 435–441.
[18] G.A. Elove, A.K. Bhuyan, H. Roder, Kinetic mechanism of cytochrome *c* folding: involvement of the heme and its ligands, Biochemistry 33 (1994) 6925–6935.
[19] W. Colon, H. Roder, Kinetic intermediates in the formation of the cytochrome *c* molten globule, Nat. Struct. Biol. 3 (1996) 1019–1025.
[20] W. Colon, L.P. Wakem, F. Sherman, H. Roder, Identification of the predominant non-native histidine ligand in unfolded cytochrome *c*, Biochemistry 36 (1997) 12535–12541.
[21] S.R. Yeh, S. Takahashi, B. Fan, D.L. Rousseau, Ligand exchange during cytochrome *c* folding, Nat. Struct. Biol. 4 (1997) 51–56.
[22] S.R. Yeh, D.L. Rousseau, Folding intermediates in cytochrome *c*, Nat. Struct. Biol. 5 (1998) 222–228.
[23] S.R. Yeh, D.L. Rousseau, Ligand exchange during unfolding of cytochrome *c*, J. Biol. Chem. 274 (1999) 17853–17859.
[24] M.M. Pierce, B.T. Nall, Coupled kinetic traps in cytochrome *c* folding: His–heme misligation and proline isomerization, J. Mol. Biol. 298 (2000) 955–969.
[25] L. Banci, I. Bertini, K.L. Bren, H.B. Gray, P. Sompornpisut, P. Turano, Three-dimensional solution structure of the cyanide adduct of a Met80Ala variant of *Saccharomyces cerevisiae iso*-L-cytochrome *c*. Identification of ligand–residue interactions in the distal heme cavity, Biochemistry 34 (1995) 11385–11398.
[26] K.L. Bren, H.B. Gray, L. Banci, I. Bertini, P. Turano, Paramagnetic ^{1}H NMR spectroscopy of the cyanide derivative of Met80Ala-*iso*-L-cytochrome *c*, J. Am. Chem. Soc. 117 (1995) 8067–8073.
[27] Y. Yao, C. Qian, K. Ye, J. Wang, Z. Bai, W. Tang, Solution structure of cyanoferricytochrome *c*: ligand-controlled conformational flexibility and electronic structure of the heme moiety, J. Biol. Inorg. Chem. 7 (2002) 539–547.
[28] L. Banci, I. Bertini, G.A. Spyroalias, P. Turano, The conformational flexibility of oxidized cytochrome *c* studied through its interaction with NH_3 and at high temperatures, Eur. J. Inorg. Chem. 5 (1998) 583–591.
[29] W. Shao, Y. Yao, G. Liu, W. Tang, ^{1}H NMR studies of pyridine binding to cytochrome *c*, Inorg. Chem. 32 (1993) 6112–6114.
[30] L. Banci, I. Bertini, G. Liu, et al., Effects of extrinsic imidazole ligation on the molecular and electronic structure of cytochrome *c*, J. Biol. Inorg. Chem. 6 (2001) 628–637.
[31] Y. Yao, C. Qian, Y. Wu, J. Hu, W. Tang, ^{1}H NMR study of 2-methylimidazole binding to cytochrome *c*: a comprehensive investigation of the role of the methyl substituent on the ligand binding affinity and heme electronic structure in imidazole–cytochrome *c* complexes, J. Chem. Soc. Dalton Trans. 12 (2001) 1841–1845.
[32] C.J. Nelson, B.E. Bowler, pH dependence of formation of a partially unfolded state of a Lys73→His variant of *iso*-L-cytochromc *c*: implications for the alkaline conformational transition of cytochrome *c*, Biochemistry 39 (2000) 13584–13594.
[33] M. Ikeda-Saito, T. Lizuka, Studies on the heme environment of horse heart ferric cytochrome *c*. Azide and imidazole complexes of ferric cytochrome *c*, Biochim. Biophys. Acta. 393 (1975) 335–342.
[34] F. Viola, S. Aime, M. Coletta, et al., Azide, cyanide, fluoride, imidazole and pyridine binding to ferric and ferrous native horse heart cytochrome *c* and to its carboxymethylated derivative: a comparative study, J. Inorg. Biochem. 62 (1996) 213–222.
[35] D. Ma, J. Lu, W. Tang, ^{1}H NMR studies of azide binding to cytochrome *c*, Biochim. Biophys. Acta 1384 (1998) 32–42.
[36] S.D. Emerson, G.N. La Mar, NMR determination of the orientation of the magnetic susceptibility tensor in cyanometnyoglobin: a new probe of steric tilt of bound ligand, Biochemistry 29 (1990) 1556–1566.
[37] D.L. Turner, Determination of haem electronic structure in His–Met cytochromes *c* by ^{13}C-NMR: the effect of the axial ligands, Eur. J. Biochem. 227 (1995) 829–837.
[38] R.O. Louro, I.J. Correia, L. Brennan, I.B. Coutinho, A.V. Xavier, D.L. Turner, Electronic structure of low-spin ferric porphyrins: ^{13}C NMR studies of the influence of axial ligand orientation, J. Am. Chem. Soc. 120 (1998) 13240–13247.

[39] R.O. Louro, M. Medina, A.P. Aguiar, et al., Structural and magnetic characterisation of the haem core of ferricytochromes c_6, J. Biol. Inorg. Chem. 3 (1998) 68–73.
[40] D.L. Brautigan, S.F. Miller, E. Margoliash, Mitochondrial cytochrome *c*: preparation and activity of native and chemically modified cytochromes *c*, Methods Enzymol. 53D (1978) 128–164.
[41] T. Inubushi, E.D. Becker, Efficient detection of paramagnetically shifted NMR resonances by optimizing the WEFT pulse sequence, J. Magn. Reson. 51 (1983) 128–133.
[42] K. Wuthrich, NMR of Proteins and Nucleic Acids, Wiley, New York, 1986.
[43] XWINNMR, version 2.6, Bruker, Rheinstetten, 2000.
[44] C. Bartels, T. Xia, M. Billeter, P. Guntert, K. Wuthrich, The program XEASY for computer-supported NMR spectral analysis of biological macromolecules, J. Biomol. NMR 5 (1995) 1–10.
[45] G.N. La Mar, J.D. Satterlee, J.S. De Ropp, Nuclear magnetic resonances in hemoproteins, in: K.M. Kadish, K.M. Smith, R. Guilard (Eds.), The Porphyrin Handbook, Academic Press, New York, 2000, pp. 185–298.
[46] M. Gochin, H. Roder, Protein structure refinement based on paramagnetic NMR shifts: applications to wild-type and mutant forms of cytochrome *c*, Protein Sci. 4 (1995) 296–305.
[47] K. Tu, M. Gochin, Structure determination by restrained molecular dynamics using NMR pseudocontact shifts as experimentally determined constraints, J. Am. Chem. Soc. 121 (1999) 9276–9285.
[48] M. Gochin, A high-resolution structure of a DNA-chromomycin-Co(II) complex determined from pseudocontact shifts in nuclear magnetic resonances, Struct. Fold. Des. 8 (2000) 441–452.
[49] L. Banci, I. Bertini, G. Gori Savellini, et al., Pseudocontact shifts as constrains for energy minimization and molecular dynamics calculations on solution structure of paramagnetic metalloproteins, Proteins 29 (1997) 6–76.
[50] L. Banci, I. Bertini, K.L. Bren, et al., The use of pseudocontact shifts to refine the solution structures of paramagnetic metalloproteins: Met80Ala cyano-cytochrome *c* as an example, J. Biol. Inorg. Chem. 1 (1997) 117–126.
[51] SYBYL, version 6.3, Tripos Inc., St. Louis, 1997.
[52] D.A. Pearlman, D.A. Case, J.W. Caldwell, et al., AMBER 5.0 Manual, University of California, San Francisco, 1997.
[53] L.L. Pearce, A.L. Gartner, M. Smith, A.G. Mauk, Mutation-induced perturbation of the cytochrome *c* alkaline transition, Biochemistry 28 (1989) 3152–3156.
[54] F.I. Rosell, T.R. Harris, D.P. Hildebrand, S. Dopner, P. Hildebrandt, A.G. Mauk, Characterization of an alkaline transition intermediate stabilized in the Phe82Trp variant of yeast *iso*-L-cytochrome *c*, Biochemistry 39 (2000) 9047–9054.
[55] L. Brennan, D.L. Turner, Paramagnetic NMR shifts in cyanoferricytochrome *c*. Investigation of thermal stability and deviations from Curie law behaviour, Biochim. Biophys. Acta. 1342 (1997) 1–12.
[56] R. Koradi, M. Billeter, K. Wüthrich, MOLMOL: a program for display and analysis of macromolecular structure, J. Mol. Graph. 14 (1996) 51–55.